Extensive cellular multitasking within *Bacillus subtilis* biofilms

Sarah M. Yannarell[1,3], Eric S. Beaudoin[2], Hunter S. Talley[3], Alexi A. Schoenborn[1,3], Galya Orr[4], Christopher R. Anderton[4], William B. Chrisler[4], Elizabeth A Shank[2,#]

[1] Department of Microbiology and Immunology, University of North Carolina at Chapel Hill, Chapel Hill, NC, USA
[2] Department of Systems Biology, University of Massachusetts Chan Medical School, Worcester, MA, USA
[3] Department of Biology, University of North Carolina at Chapel Hill, Chapel Hill, NC, USA
[4] Environmental Molecular Sciences Laboratory, Pacific Northwest National Laboratory, Richland, WA, USA

[#] Corresponding Author
Email: Elizabeth.Shank@umassmed.edu

Running Title: Heterogeneity in *Bacillus subtilis* biofilms

ORCIDs:

Sarah M. Yannarell:	0000-0003-4504-9193
Eric S. Beaudoin:	0000-0003-1104-4538
Hunter S. Talley:	0000-0003-4801-1158
Alexi A. Schoenborn:	0000-0003-2998-638X
Galya Orr:	0000-0002-5552-2151
Christopher R. Anderton:	0000-0002-6170-1033
William B. Chrisler:	
Elizabeth A. Shank:	0000-0002-4804-1966

Address Correspondence to: Elizabeth A. Shank, Elizabeth.Shank@umassmed.edu, 774-455-6624, 368 Plantation St., ASC-5.1059, Worcester, MA 01605

Keywords: biofilms, cell-types, confocal microscopy

Contributions:

Conceptualization	SY, EAS	Resources	SY, HT, AS
Data Curation	SY, WC	Software	EB
Formal Analysis		Supervision	EAS, CA, WC, GO
Funding	EAS, SY	Validation	SY, WC
Investigation	SY, EB, WC, HT	Visualization	SY, EAS, EB
Methodology		Writing-original	SY
Proj Admin	EAS, GO	Writing-editing	SY, EAS

ABSTRACT

Bacillus subtilis is a soil-dwelling bacterium that can form biofilms, or communities of cells surrounded by a self-produced extracellular matrix. In biofilms, genetically identical cells often exhibit heterogeneous transcriptional phenotypes so that only subpopulations of cells carry out essential yet costly cellular processes that allow the entire community to thrive. Surprisingly, the extent of phenotypic heterogeneity and the relationships between subpopulations of cells within biofilms of even in well-studied bacterial systems like *B. subtilis* remains largely unknown. To determine relationships between these subpopulations of cells, we created 182 strains containing pairwise combinations of fluorescent transcriptional reporters for the expression state of 14 different genes associated with potential cellular subpopulations. We determined the spatial organization of the expression of these genes within biofilms using confocal microscopy, which revealed that many reporters localized to distinct areas of the biofilm, some of which were co-localized. We used flow cytometry to quantify reporter co-expression, which revealed that many cells 'multi-task', simultaneously expressing two reporters. These data indicate that prior models describing *B. subtilis* cells as differentiating into specific cell-types, each with a specific task or function, were oversimplified. Only a few subpopulations of cells, including surfactin and plipastatin producers, as well as sporulating and competent cells, appear to have distinct roles based on the set of genes examined here. These data will provide us with a framework with which to further study and make predictions about the roles of diverse cell phenotypes in *B. subtilis* biofilms.

IMPORTANCE

Many microbes differentiate, expressing diverse phenotypes to ensure their survival in various environments. However, studies on phenotypic differentiation have typically examined only a few phenotypes at one time, thus limiting our knowledge about the extent of differentiation and phenotypic overlap in the population. We investigated the spatial organization and gene expression relationships for genes important in *B. subtilis* biofilms. In doing so, we mapped spatial gene expression patterns and expanded the number of cell populations described in the *B. subtilis* literature. It is likely that other bacteria also display complex differentiation patterns within their biofilms. Studying the extent of cellular differentiation in other microbes may be important when designing therapies for disease-causing bacteria, where studying only a single phenotype may be masking underlying phenotypic differentiation relevant to infection outcomes.

INTRODUCTION

Bacterial communities exist across diverse ecosystems. In these communities, genetically identical bacterial cells undergo differentiation that results in transcriptionally and functionally distinct cellular phenotypes (1). Such differentiation can result from nutrient availability (2), interspecies coculture interactions (3), stochastic effects (4), or specific microenvironments (5). It is thought that cells differentiate into phenotypically distinct subpopulations as a community survival strategy (2, 6-8). For many bacteria, the resulting phenotypic heterogeneity among genetically identical cells has implications for surface sensing (9, 10), virulence (11-13), and metabolism (14). For instance, some cell subpopulations may specialize in sugar incorporation (15) while others may release metabolic products (16). There is evidence of cross-feeding between glucose-fermenting and acetate-respiring subpopulations in *Escherichia coli* (17) and coordination between cells from the interior and periphery of *Bacillus subtilis* colony biofilms (18). Phenotypic differentiation is also implicated in antibiotic tolerance: *Pseudomonas aeruginosa* exhibits heterogeneity in its cellular metabolism due to oxygen gradients, which impacts how cells respond to antibiotics (19, 20). In *B. subtilis*, distinct subpopulations produce energetically costly compounds, like extracellular matrix components (21), extracellular proteases (22), or surfactin (23). This division of labor may have ecological benefits, since surfactin reduces surface tension to allow migration across solid surfaces (24) and extracellular matrix promotes plant root adherence (25).

Given these potential incentives for cellular differentiation, phenotypic heterogeneity is a hallmark of bacterial biofilms, which are complex communities of cells encased by a self-produced extracellular matrix (26). Many models of cellular differentiation exist, but *Bacillus subtilis* is one of the best characterized, as well as being a genetically tractable, biofilm-forming bacterium (27). Based on the current (limited) fluorescent transcriptional reporter data available in the literature, *B. subtilis* is described as differentiating into six cellular phenotypes, leading to cells that are motile, matrix-producing, sporulating, cannibal, protease-producing, and competent (28) (Table 1). This model was derived based on data from fluorescent transcriptional reporters that use the expression of a marker gene as a proxy for the cell's transcriptional state (e.g., a flagellar protein is a marker for motility), with heterogeneous gene expression leading to the designation of these cell types. Furthermore, the explicit examination of phenotypic overlap of these putative cell-types has been conducted in only a handful of cases (29-34). These studies indicate that motile, matrix-producing, and sporulating cells are spatiotemporally distinct within biofilms, as are matrix-producing cells from those that are competent or are producing the specialized metabolite surfactin. In contrast, matrix-producing and cannibal cells appear overlapping (23) and matrix-producing and protease-producing genes are co-expressed at certain times during growth (35). Beyond these few studies, the relationships between most other described cellular subpopulations in *B. subtilis* are unknown.

In addition to these six canonical cellular phenotypes, metabolite-producing cell subpopulations also play important roles in *B. subtilis* biofilm communities (36-38). *B.*

subtilis NCIB3610 produces at least ten specialized metabolites, some of which act as cell-cell communication molecules and impact cellular differentiation (39). For instance, surfactin is a key factor in the formation of biofilm-matrix-producing cells (30, 39, 40), while ComX has been shown to stimulate the expression of surfactin through a ComP-ComA signaling cascade (41, 42). Of the remaining *B. subtilis* metabolites, four others have had intraspecific signaling bioactivities ascribed to them (23, 39, 40, 43, 44). While the expression of a handful of these metabolites have been previously examined for heterogeneous expression patterns in *B. subtilis* (23, 30, 45-50), only three of these have been examined within *B. subtilis* colony biofilms (23, 30, 50, 51), and even fewer have been examined in terms of their spatial organization (50). Thus, our understanding of the gene expression relationships between these specialized metabolites and the other described *B. subtilis* phenotypes is largely fragmentary, with many studies using cells grown under inconsistent growth conditions. Here we aim to examine the expression patterns of all ten metabolite biosynthetic genes and six currently described phenotypic cell-types under uniform biofilm-inducing conditions to obtain insights into the putative roles of these metabolites as cell-cell differentiation signals within *B. subtilis* model biofilms.

Considering the many described cell-types and metabolites known to exist within *B. subtilis* biofilms, the studies described above highlight that currently an incomplete understanding of *B. subtilis* cellular heterogeneity exists. We predict, based on the diverse gene expression relationships described so far, that substantial additional transcriptional multi-tasking occurs within *B. subtilis* biofilms. Here we aim to determine

the extent of both transcriptional multi-tasking and the phenotypic cellular coordination within *B. subtilis* biofilms using single and pairwise fluorescent transcriptional reporters for genes previously associated with specific cell-types or specialized metabolites. Using flow cytometry and fluorescence microscopy, we quantitatively measured the expression overlap between the expression of these genes within individual cells as well as visualizing their spatial distributions within *B. subtilis* biofilms. Overall, we determined that some genes examined here were only expressed in a small subset of cells, while other cells multi-task, expressing multiple genes simultaneously. In addition, we observed that, overwhelmingly, most of the genes examined were expressed in distinct and repeatable spatial patterns across the biofilm. The data presented here thus provides a substantially improved, more comprehensive model of cellular heterogeneity within *B. subtilis* biofilms than currently exists.

RESULTS

Heterogeneous *B. subtilis* gene expression at the colony level

To monitor *B. subtilis* gene expression over time and space, we constructed strains containing fluorescent transcriptional reporters for key *B. subtilis* genes. To do this, we introduced the fluorescent protein Ypet (a variant of yellow fluorescent protein) under the control of promoters for 15 genes of interest (Table 1) and incorporated them into the neutral *amyE* locus (52). These genes are involved in specialized metabolite production, extracellular matrix production, motility, sporulation, competence, protease production, and cannibal antibiotic production. Exploring this wide range of genes was

intended to provide a more global view of cellular phenotypic variation in *B. subtilis* than previously examined. We initially looked at the fluorescent transcriptional reporters for all ten of the specialized metabolites but excluded sublancin from future experiments because initial results showed that its colony morphology differed from that of wild type (Figure S1); we therefore focused on 14 *B. subtilis* genes.

To obtain information about the relationships between the expression of these genes, we first asked how the expression of these fluorescent transcriptional reporters were localized and how intensely they expressed *YPet* within *B. subtilis* biofilms. We grew biofilm colonies from an OD_{600}-normalized inoculum on MSgg, a *B. subtilis* biofilm inducing media (53), and imaged colonies at 48 h (Figure 1) using brightfield and fluorescence illumination. We calculated the average fluorescence intensity across the colony, averaged from the center outward (Figure S2). At the colony level, we observed a range of reporter expression patterns. Two metabolite reporters (*sdpA* and *sboA*) were expressed at high levels; eight reporters (for genes encoding metabolite or structural products: *bacA, tapA, skfA, dhbA, comQX, hag, pksC,* and *sspB*) were expressed at mid-range levels; and the reporters for four genes (*ppsA, srfAA, comGA,* and *aprE)* were expressed at low or at near-background levels (Figure 1, Figure S2). With regards to their localization, the *sdpA, bacA, comQX, ppsA, srfAA*, and *aprE* reporters seemed to be consistently expressed throughout the colony (Figure 1, Figure S2). In contrast, *hag, sboA, dhbA,* and *pksC* were expressed primarily in the interior of the colony while t*apA*, *skfA*, and *sspB* were expressed mostly in the periphery (Figure 1, Figure S2). Thus, in comparing the fluorescence localization of different reporters at the

colony level, we already observed some genes with similar spatial expression patterns and others with distinct expression patterns.

Identifying colony-level gene expression relationships using double-labeled strains

We hypothesized that the areas of the *B. subtilis* colony that appeared to be expressing more than one fluorescent transcriptional reporter could either be composed of highly heterogeneous populations of cells or else individual cells in those regions could be expressing multiple genes simultaneously, i.e., multitasking. To better visualize and quantify gene expression co-localization within *B. subtilis* colonies, we generated strains that contained pairwise combinations of these 14 reporters at two neutral sites on the *B. subtilis* chromosome (one reporter at the *amyE* locus (52) and the other at the *lacA* locus (54)) using phage transduction (Figure 2A). In combining reporter constructs for the 14 genes of interest, we created 182 strains; this included all 91 possible pairwise combinations of the 14 genes in each of the two color orientations (e.g., both P_{hag}-*YPet*::*amyE*, P_{tapA}-*mTurq*::*lacA* and P_{tapA}-*YPet*::*amyE*, P_{hag}-*mTurq*::*lacA* to control for differences in fluorescent protein expression levels). Only six such dual-reporter strain pairs (*hag-tapA*; *hag-sspB*; *tapA-sspB*; *srfAA-tapA*; *skfA-tapA*; and *tapA-comGA*) have been explicitly examined in the literature previously (23, 29, 30, 32, 33). All strains containing dual reporters grew similarly to wild-type *B. subtilis* (Figure S3). In analyzing the fluorescence levels of colony biofilms of these strains, we built a comprehensive picture of the spatial expression relationships between each of these gene pairs. We did so by growing the dual-reporter stains on MSgg and visualizing fluorescence within

176 colonies at 48 h to directly compare expression patterns. In some pairs, like *sdpA*
177 (cannibal) and *skfA* (cannibal), we observed high levels of co-localization (indicated by
178 white in false-colored overlay image) (Figure 2B). Conversely, a *B. subtilis* strain
179 containing *tapA* (matrix-producing) and *sboA* (subtilosin) reporters exhibited little co-
180 localization between the expression of these two genes (Figure 2C).
181
182 **Analyzing gene expression in stratified, thin-sectioned colonies by confocal**
183 **microscopy**
184 The colony-level fluorescence microscopy allowed us to identify areas of the colony that
185 appeared to contain co-localized reporter gene expression. We then delved further into
186 this potential co-expression of genes using a confocal-laser-scanning microscope
187 (CLSM) with an Airyscan detector. To gather spatial information not only from the
188 surface of the colony, but also from individual cells within the biofilm, we quartered and
189 thin-sectioned the colonies to 20 μm thick and flipped the sections on their side for
190 imaging (schematic shown in Figure 3A). This approach enables a finer spatial
191 visualization of fluorescence expression patterns within the depth of biofilms and
192 provides information about the distributions of cells expressing different genes across
193 the structure. For example, both *sdpA* (cannibal) and *skfA* (cannibal) reporters are
194 present throughout the interior and peripheral regions of the colony and the reporters
195 seem fairly well mixed in these regions, with some cells co-expressing both fluorescent
196 reporters (white cells in Figure 3B). In contrast, *sboA* (subtilosin) and *tapA* (matrix-
197 producing) are predominantly localized to the interior and the periphery, respectively,
198 and these reporters seem to be mutually exclusive in individual cells (Figure 3C).

199

200 **Flow cytometry to quantify gene expression within individual cells**

201 While the results from CLSM provided information about the spatial organization of
202 gene expression across *B. subtilis* biofilm colonies, these data were not quantitative and
203 in some cases it remained ambiguous whether (and the extent to which) genes were
204 being co-expressed in the same cell. Therefore, we used flow cytometry to quantify
205 gene expression and co-expression within *B. subtilis* biofilm cells using our double-
206 labeled strains. We harvested colonies of all 182 dual-reporter strains grown on MSgg
207 and fixed the cells using paraformaldehyde to prevent changes in expression levels
208 during processing. Samples were sonicated, filtered, and analyzed on a flow cytometer,
209 where data from a minimum of 24,000 cells per strain were collected.

210

211 We used *B. subtilis* non-fluorescent control samples to set the flow cytometry
212 fluorescence detection gates, which enabled us to differentiate cell populations from
213 each strain that were: a) not expressing either fluorophore, b) only expressing *mTurq*, c)
214 only expressing *Ypet*, or d) expressing both fluorophores (Figure S4) To understand
215 how many cells in the overall biofilm were expressing each individual gene, we first
216 quantified the total percentage of cells expressing *Ypet* from each strain (Figure 4A).
217 (We used only the *Ypet* signal from each dual-labeled strain for these calculations since
218 the sensitivity of this fluorescent protein was superior to *mTurq* due to cellular
219 background fluorescence in the *mTurq* channel). With this analysis, we determined that
220 most cells within the *B. subtilis* population express *sdpA*, *comQX,* and *skfA,* while very

221 few express *ppsA*, *srfAA*, or *comGA* (Figure 4A). The remaining eleven genes were
222 expressed in between 25 - 75% of the cell population.
223
224 To understand the expression relationships between all of these genes, we then
225 quantified the proportion of cells that expressed both *mTurq* and *Ypet* in each dual-
226 labeled strain. We observed a range of gene-expression relationships, from completely
227 distinct to fully overlapping (Figure 4B; all flow cytometry plots can be found in the
228 Supplementary material (Figure S4)). Our dataset includes reporter pairs that
229 corroborate results from previous studies (e.g., motility (*hag*) and sporulation (*sspB*)
230 were not co-expressed (29) and biofilm matrix (*tapA*) and *skfA* (cannibal) reporters were
231 overlapping (55)). However, in our data set, ~45% of the population co-express *tapA*
232 and *sspB* reporters, which were originally described as distinct cell-types (29).
233 Unexpectedly, *sdpA* did not appear to be coregulated with *tapA*, even though *tapA* is
234 highly co-expressed with *skfA*, the other *B. subtilis* cannibalism toxin. Another
235 unanticipated finding was that *comGA*, *ppsA*, and *srfAA* had minimal expression overlap
236 with any other genes (Figure 4B) (with the exception of *sboA*, which was expressed in
237 nearly all cells), indicating that cells expressing these genes may indeed represent more
238 distinct cell-types that are specializing in a particular task. Beyond this, although most
239 genes demonstrated some expression overlap with other genes (Figure 4B), some pairs
240 of genes appeared to have anticorrelated expression: *sspB* and *dhbA, sspB* and *aprE,*
241 *sspB* and hag, as well as *hag* and *aprE, hag* and *comQX*, *skfA*, and *pksC* (Figure 4B).
242
243 **Correlating the flow cytometry to microscopy**

The flow cytometry results revealed extensive multitasking occurring in *B. subtilis* biofilm cells. However, by nature these flow cytometry data lack spatial information. We next wanted to investigate how cells expressing particular genes or gene pairs were spatially distributed within the colony. To do so, we used confocal microscopy to visualize representative reporter pairs with distinct flow cytometry distributions. In Figure 5 we show some examples of the diverse co-expression patterns we observed. For example, the flow cytometry data from the *sdpA*-*sboA* reporter pair indicate that almost all *sboA*-expressing cells also express *sdpA* (Figure 5A). In addition, however, there is a subset of *sdpA*-only expressing cells (Figure 5A, yellow bracket), and the cells expressing both reporters have a bimodal expression, where some express *sboA* at lower levels (Figure 5A, blue bracket), and others at very high levels (Figure 5A, red brackett). Interestingly, the spatial organization of these subpopulations of cells is not random: the brighter *sboA* population correlates with cells exhibiting higher expression at the colony agar interface (Figure 5D), while the *sdpA*-only subpopulation of cells are found at the colony-air interface (Figure 5D).

The *sspB* gene, a reporter for sporulation that is expressed during the first committed step of sporulation, exhibited an unusual, bimodal expression pattern. The *sspB* reporter was either on or off (Figure 5B). This is consistent with sporulation being known to be an all-or-none process at the stage at which the *sspB* gene is expressed; at 48 h of biofilm growth on MSgg we know that a subset of the population has begun to sporulate (29). The cells expressing *sspB* are also small and punctate in our fluorescence micrographs, indicative of cells undergoing sporulation (Figure 5E) (56,

57). In this field of view, we see little overlap with *bacA* (bacilysin)-expressing cells, which corresponds to the lower right quadrant of the flow cytometry data (Figure 5E); cells co-expressing *bacA* and *sspB* must reside elsewhere in the colony, since they are not visible here (Figure 5E).

Lastly, for a handful of reporters, we observed a partially overlapping gene expression pattern in our flow cytometry data (e.g., Figure 4B). The flow cytometry plot for reporter pair *dhbA* (bacillibactin) and *pksC* (bacillaene) displays this partial overlap, with each reporter expressed alone in a subset of cells as well as in some cells simultaneously (Figure 5C). Regions of co-localization in the center interior of the biofilm correlate to the observed co-expression in flow cytometry data (Figure 5F).

Correlating reporters to each other using microscopy

We then examined the spatial relationships between different fluorescent reporters within each reporter strain of *B. subtilis* based on the confocal fluorescence micrographs. This was done as a voxel-based analysis using BiofilmQ (58). Voxels were 10 cubic pixels, or about 0.80 μm per side. Pearson correlation coefficients were derived for each voxel by looking at the intensity of each of the two reporters. Each Pearson value was overlaid onto the centroid location of the voxel. We saw that a range of distinct relationships were present (Figure 6) between different reporter pairs, supporting the diversity of relationships present between each set of genes as observed in the flow cytometry data. The expression of *sspB* and *sboA* were anti-correlated, while *pksC* and *bacA* expression was correlated in the center and on the edge of the biofilm.

Interestingly, *pksC* and *dhbA* expression was correlated in the center but somewhat anticorrelated in the periphery, suggesting that a *pksC*- and *dhbA*-active cell-type is present in the center of the biofilm. These cross-sections provide an even more nuanced view of how different gene pairs are related to one another throughout the biofilm colony.

DISCUSSION

Historically, researchers have classified *B. subtilis* into several cell states or subpopulations that were identified based on the gene expression inferred by a handful of fluorescent transcriptional reporters (36). In this study, we have built upon these foundational studies and generated 182 strains containing all pairwise combinations (91 reporter pairs in both color combinations) of a suite of 14 fluorescent transcriptional reporters that report on the gene expression of described cell physiologies as well as genes that encode specialized metabolite machinery in *B. subtilis*. By analyzing the spatial and co-expression relationships of genes controlling these critical phenotypes and the production of cell-cell metabolite signals within *B. subtilis* biofilms, we have uncovered which genes are simultaneously expressed within *B. subtilis* cells, enhancing our understanding of how extensively cells within these biofilm communities are multitasking. Furthermore, the expression patterns of these genes are spatially distributed in a repeatable way across biofilms (shown here and in (50)). Our ambitious evaluation of these many strains by both flow cytometry and microscopy has led to a

312 substantially more nuanced and thorough view of cellular heterogeneity within *B. subtilis*
313 biofilms.
314
315 Our study reveals a substantial level of multitasking within *B. subtilis* biofilm cells. We
316 frequently observed subpopulations of cells that co-expressed two reporters as well as
317 subpopulations that only expressed one of the two reporters (Figure 4). Our data
318 indicate that 66% (60/91) of the phenotypes examined here are co-expressed in at least
319 some *B. subtilis* biofilm cells (Figure 4F). Given the diverse reasons cells differentiate
320 (e.g., division of labor in producing extracellular matrix or in generating cells tolerant to
321 antibiotics, etc.), it is possible that *B. subtilis* cells may multitask to provide an additional
322 layer of 'bet-hedging' in the face of environmental stress. Further work interrogating the
323 broader, genome-wide gene expression patterns of individual cells within biofilms would
324 be informative here. The global transcriptome of *B. subtilis* has been analyzed
325 previously (59, 60), but data about the specific transcriptional profile of multitasking cells
326 are masked when biofilms are harvested and analyzed in bulk. Previous studies have
327 coupled fluorescence-activated cell sorting followed by RNA sequencing to examine
328 competent (*comG*+) and non-competent subpopulations (61) and succinate co-A ligase
329 (*sucC*+) populations (16) in *B. subtilis*. We anticipate using such approaches, in
330 conjunction with our suite of dual-labeled fluorescent reporter strains, to isolate and
331 determine the transcriptome of specific subpopulations of *B. subtilis* cells. Expanding
332 the current collection of reporters to include other genes implicated in cell-cell
333 communication and biofilm formation (62-65) would provide an even more refined view
334 of cellular transcriptional heterogeneity within bacterial biofilms.

Similar to how the spatial arrangements of bacteria in multispecies biofilms impact the function and bioactivities of these communities (66-72), we expect that in single-species biofilms the spatial organization of cellular subpopulations (as defined by their distinct gene expression profiles) may also be important for the function of differentiated cells. The organization of cells with specific gene expression patterns may also provide clues about the underlying regulation of these genes. We expect that genes expressed in distinct locations across the biofilm may indicate that their expression is regulated by microenvironmental factors. For instance, the organization of *sdpA* and *sboA* reporters (Figure 4B) may indicate that *sdpA* expression is important for all cells, while *sboA* expression is more important near the agar; conversely, it may be important that *sboA is* not expressed at the top of the biofilm. In contrast, when two reporters are expressed in the same location but in different cells, for instance *pksC* and *dhbA* (Figure 4D), we predict that their regulation may not be microenvironment-specific but could instead be stochastic or directed by a positive feedback loop (73). A technique developed to use stochastic pulsing force the expression of genes typically not co-expressed (74) could be applied to investigate the underlying regulation of co-localized reporters in biofilms and determine the functional effects of dysregulated gene expression. Mutations could similarly be used to dysregulate gene expression; mutants in motility-related genes (*hag, cheA, cheY*) have been seen to alter the expression of *hag* (using a P_{hag}-*yfp* reporter) (29).

B. subtilis and many other bacteria dedicate a large portion of their genome to specialized metabolite gene clusters (75, 76); many of the metabolites produced by these biosynthetic genes act as cell-cell signals (77). Many of the biosynthesis genes for specialized metabolites examined here were co-expressed and co-localized with other specialized metabolite and physiological reporter genes. This overlap suggests that the gene expression of the biosynthesis machinery for generating specialized metabolites such as subtilosin, bacillaene, bacillibactin, and comX are co-expressed with (and potentially regulate the generation of) cellular phenotypes such as matrix-production, cannibalism, and extracellular protease production. Other genes that exhibited minimal gene expression overlap (such as those for motility, sporulation, competence, plipastatin, and surfactin) may have more specific roles in the biofilm. Our work greatly advances our understanding of which cells within a biofilm express specialized metabolite biosynthesis genes, but only by using techniques that directly detect metabolites, such as our recent study using mass spectrometry imaging (50), are able to resolve how far these metabolites signals physically diffuse from the producing cells. Modeling approaches that are able to integrate all of these diverse datasets (microscopy, quantitative flow cytometry, mass spectrometry imaging) may enable us to generate a comprehensive and predictive spatial model of specialized metabolite signaling in bacterial biofilms.

This work greatly advances our understanding of the heterogeneity of cellular gene expression and transcriptional multitasking that exists within the biofilms of the model bacterium *B. subtilis*. The spatial transcriptional complexity we describe here within this

single-species biofilm is likely to be further modified by interactions with other bacteria and fungi. We know that multiple other bacteria can affect *B. subtilis* physiology based on single-gene reporter constructs (44, 78, 79) and predict that these changes are representative of shifts in the balance of transcriptional heterogeneity that are propagated across many other genes. The tools and approaches we implemented here could similarly be utilized to address the question of cellular transcriptional heterogeneity within multispecies communities and how their spatial organization may shift in response to environmental stressors. This research, which provides an unusually complete depiction of how *B. subtilis* differentiates within biofilms, provides a foundation for exploring more complex metabolic and regulatory interactions between cells within environmentally and agriculturally important microbial communities.

ACKNOWLEDGEMENTS

We gratefully acknowledge the assistance and advice of Srigokul (Gokul) Upadhyayula (UCBerkeley) on the image processing, troubleshooting, and computational analysis performed in this paper. This research was supported by funds provided by the National Institutes of Health (GM112981 to E.A.S.) A portion of this research was performed on a project award (10.46936/expl.proj.2019.51105/60000139) from the Environmental Molecular Sciences Laboratory, a DOE Office of Science User Facility sponsored by the Biological and Environmental Research program under Contract No. DE-AC05-76RL01830. Some of this material is based upon work supported by the U.S. Department of Energy, Office of Science, Office of Workforce Development for

Teachers and Scientists, Office of Science Graduate Student Research (SCGSR) program (to S.M.Y). The SCGSR program is administered by the Oak Ridge Institute for Science and Education (ORISE) for the DOE. ORISE is managed by ORAU under contract number DE-SC0014664. All opinions expressed in this paper are the author's and do not necessarily reflect the policies and views of NIH, DOE, ORAU, or ORISE.

MATERIALS AND METHODS

Bacterial strains and growth conditions. Table S1 lists the strains used in this study. *B. subtilis* strains were cultured on lysogeny broth (LB)-Lennox medium (10 g/liter tryptone, 5 g/liter yeast extract, 5 g/liter NaCl, 1.5% agar) at 30 °C for 16 to 18 h with antibiotics as necessary. TY broth consisted of LB supplemented with 10 mM $MgSO_4$ and 100 µM $MnSO_4$ after autoclaving. Colony biofilms were grown on MSgg medium (5 mM potassium phosphate [pH 7], 100 mM morpholinepropanesulfonic acid [MOPS; pH 7], 2 mM $MgCl_2$, 700 µM $CaCl_2$, 50 µM $MnCl_2$, 50 µM $FeCl_3$, 1 µM $ZnCl_2$, 2 µM thiamine, 0.5% glycerol, 0.5% glutamate) at with 1.5% agar at 30 °C for 48 h. Antibiotics (final concentrations) were as follows unless noted otherwise: MLS (1 µg/ml erythromycin, 25 µg/ml lincomycin) and chloramphenicol (5 µg/ml). *Escherichia coli* strains were cultured in LB-Miller medium (10 g/liter tryptone, 5 g/liter yeast extract, 10 g/liter NaCl, 1.5% agar). Final concentration of carbenicillin was 50 µg/ml.

Colony morphology phase contrast and fluorescence imaging. Macrocolony biofilm images were gathered using a Zeiss SteREO Discovery.V8 dissecting

stereomicroscope (Zeiss, Oberkochen, Germany) with a 1 × 0.63 lens objective in three channels: brightfield, Ypet, and mTurq. Images were exported to as a .TIFF for image analysis at 1388 × 1040 pixels. These images were indexed and grouped based on the strain and reporters the strain contained. Images were then imported into Matlab 2020b. For each strain, the location of the colony was determined by masking the image using the Laplassian of Gausian of a grayscale brightfield image. This method of detection was used because the agar was a single, relatively uniform value, while the colony was a substantially different, relatively uniform value. The center of the colony was determined using the Centroid function in Matlab. The edge of the colony was determined using bwboundries function in Matlab on the masked colony image. The average Euclidian distance, in number of pixels, between the center and edge of the colony was then determined. Each pixel's "Euclidian distance from the center of the colony" was divided by the "average Euclidian distance from the center of the colony to the edge," transforming each pixel's distance into a percentage (with the edge of the colony being 100%) to allow for easier comparison between colony images. Each distance was rounded to two decimal places, then the mean signal in mTurq and Ypet was taken for each unique distance at and graphed. Graphs were limited to 120% on the X-value to capture background fluorescence just beyond the edge of the colony. Y-values were normalized to an appropriate and consistent value for each reporter. The code can be found at DOI: 10.5281/zenodo.4624987.

SPP1 phage transduction. Phage transduction was carried out as previously described (80). Briefly, we grew the *B. subtilis* donor strain at 37 °C in TY broth until the

culture reached an OD_{600} of 1.0. At that point, we infected cells with SPP1 phage stock and incubated for 15 min at 37 °C. We then added 0.5% TY soft top agar to the cells and phage, overlaid the mixture on TY 1.5% agar plates, and incubated plates at 37 °C for 8 to 16 h. *B. subtilis* donor phage plaques were collected and pelleted using a clinical centrifuge. We infected *B. subtilis* recipient cells with three hundred microliters of supernatant, and then plated the cell lysate on LB-Lennox with 10 mM citrate and antibiotic to which the donor strain was resistant. Plates were incubated at 37 °C for 12 to 24 h. Four colonies were picked from each phage transduction and struck on LB-Lennox plates with antibiotic. After growth, strains were restruck two more times on LB-Lennox plates with antibiotic. Cells were spotted on MSgg and incubated at 30 °C to ensure growth, which indicates the cells have a 3610 rather than a 168 background (which is an amino acid auxotroph). Specifics of reporter construction are described below.

Construction of *B. subtilis* reporter strains. The newly constructed transcriptional reporter plasmids (pES099 – pES112) containing *Ypet* were derived from pES045 (*amyE::*P_{spacC}-*Ypet*) (81, 82). To construct these plasmids, the *spacC* promoter was removed by digestion with EcoRI and HindIII and replaced with promoter sequences. Promoter sequences were amplified from *B. subtilis* wild-type genomic DNA (See primers in Table S1) and inserted into the base plasmid by isothermal assembly (also used for all subsequent constructions described in this section) (83) and transformed into *E. coli.*

A plasmid containing mTurquoise2 (*mTurq*) was generated using primer ES395 and primer ES315 (see Table S1) to amplify *mTurq* from GL-FP-31. The fragment was cloned into plasmid pDR183 [*lacA*::(*mls*)] (84) digested with SalI and EcoRI. To create *mTurq* reporters, we amplified promoter sequences from *B. subtilis* wild-type genomic DNA (see primers in Table S1), digested with NheI and SalI, and inserted into the pDR183-*mTurq* base plasmid (pES069) using Isothermal assembly. The assembled plasmids were transformed into *E. coli.*

Upon final construction, the plasmids were isolated from *E. coli*, linearized, and transformed into *B. subtilis* 168 cells grown to stationary phase. Cells containing *Ypet* reporters were plated on Lennox-chloramphenicol to select for transformants. Cells containing *mTurq* reporters were plated on Lennox-MLS to select for transformants. Phage transduction was carried out as described previously (80) and above. *B. subtilis mTurq* reporters were used as the donor strains and grown to 37 °C in TY broth until the culture reached an OD_{600} of 1.0. Cells were infected with SPP1 phage stock and plated on 0.5% TY soft top agar, overlaid on TY 1.5% agar plates, and incubated at 37 °C for 8 to 16 h. *B. subtilis* donor phage plaques were collected and pelleted using a clinical centrifuge. Three hundred microliters of supernatant was used to infect *B. subtilis* 3610 wild-type and *B. subtilis Ypet* reporter strains (recipient cells) to construct single and dual-fluorescent reporters, respectively. The cell lysate was then plated on LB-Lennox with 10 mM citrate and MLS to which the donor *mTurq* reporter strains were resistant. Plates were incubated at 37 °C for 12 to 24 h. Three colonies were picked from each phage transduction and struck on LB-Lennox plates with MLS and citrate to select for *B.*

494 *subtilis* cells that contained *mTurq* reporters. For strains containing dual-fluorescent
495 reporters, strains were then re-struck on Lennox-chloramphenicol to select for strains
496 containing both *mTurq* and *Ypet* reporters. Cells were spotted on MSgg and incubated
497 at 30 °C to ensure growth, which indicates the cells have a 3610 rather than a 168
498 background (which is an amino acid auxotroph). Colony morphology of reporter strains
499 were compared to wild type, as morphology should be identical.
500
501 **Flow cytometry.** *B. subtilis* strains were prepared and grown on MSgg as described
502 above. After 48 h of growth, biofilms were collected and resuspended in 1 mL 1X
503 phosphate buffered saline (PBS) using a 23G needle and syringe to shear the biofilm.
504 Cells were pelleted by centrifugation at 16,000 x g, the supernatant was removed, and
505 the cells were fixed in 200 µL of 4% (w/v) paraformaldehyde for 7 minutes. After the
506 incubation, the cells were pelleted, washed in 1X PBS to remove residual
507 paraformaldehyde, and resuspended in GTE buffer [1% glucose (wt/vol) and 5 mM
508 EDTA in 1× phosphate buffer, pH 7.4]. Samples were stored at 4 °C until flow cytometry
509 analysis. Prior to analysis, cells were sonicated for 12 pulses [1 s pulse with subsequent
510 1 s pause] and filtered through a 38-µm nylon mesh. *Ypet* and *mTurq* fluorescence in
511 dual-reporter strains was measured using the 488 and 457 lasers, respectively, of the
512 Influx cell sorter (BD Biosciences).
513
514 **Thin-sectioning.** The thin-sectioning protocol was adapted from Vlamakis et al. and
515 Marlow et al (29, 35). *B. subtilis* strains were cultured on MSgg as described above and
516 vapor fixed with 8% paraformaldehyde (adapted from (85)). Biofilm-agar blocks were

quartered, transferred to a 15 x 15 x 5 mm mold (Fisher; Cat: 22-363-553), and snap-frozen. The colony was then overlaid with 4% (w/v) agarose (Lonza; Cat: 50181) and frozen at -80 °C for 15 min. The blocks were transferred to -20 °C for 30 min to equilibrate. Colony blocks were mounted to the chuck with double-distilled H_2O and sliced to 20 µm thick cross-sections using a cryotome (Thermo cryostar NX70). Sections were attached to VWR Superfrost Plus slides (Cat: 48311-703), and stored at -20 °C.

Confocal microscopy and image analysis. Sections for microscopy were overlaid with mounting medium ProLong Gold Antifade Mountant (ThermoFisher; Cat: P10144) unless otherwise noted and a 25 x 25 mm coverslip (Fisher; 12-548-C). Sections were imaged using a Zeiss 710 laser scanning confocal microscope equipped with a 20X EC Plan NEOFLUAR and 100X Plan APOCHROMAT oil objective.

DATA AVAILABILITY

The code for spatial quantification of fluorescence over the bacterial colonies can be found at DOI: 10.5281/zenodo.4624987. Images of all flow cytometry plots are available in the supplemental material section as Figure S4. All raw microscopy images will be uploaded onto Dryad.com (currently in process).

538 **TABLES**

Gene	Phenotype
aprF	Protease
bacA	Bacilysin
comG	Competence
comQ	Pheromone
dhbA	Bacillibactin
hag	Motility
pksC	Bacillaene
ppsA	Plipastatin
sboA	Subtilosin
sdpA	Cannibal (SDP)
Skf	Cannibal (SKF)
skfAA	Surfactin
sspB	Sporulation
sunA	Sublancin
tapA	Biofilm

Table 1. *B. subtilis* phenotypes and corresponding genes

550

551

552 **FIGURES AND FIGURE LEGENDS**

553

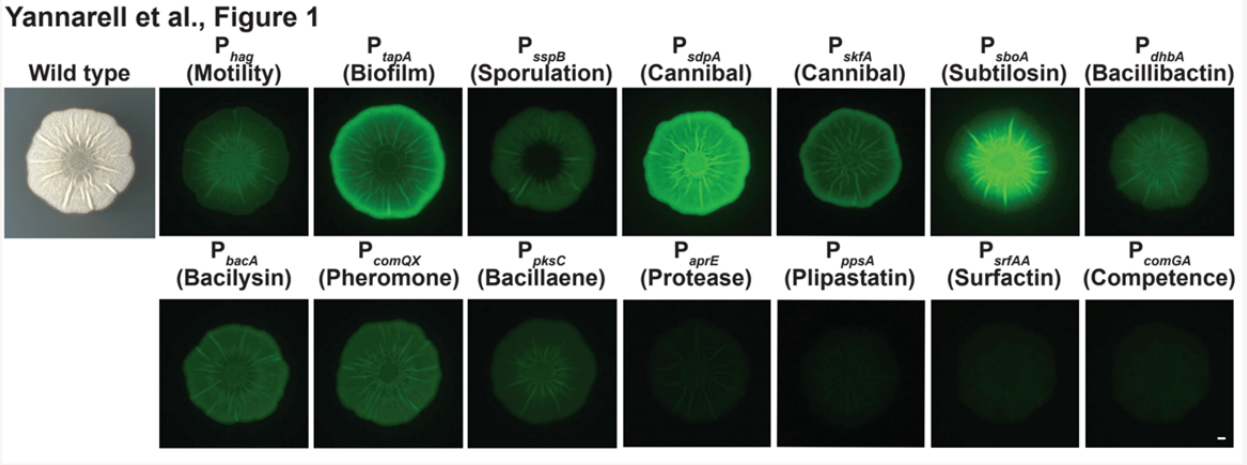

554

555 **Figure 1. *B. subtilis* exhibits heterogeneous gene expression patterns at the**

556 **colony level.** Wild-type *B. subtilis* and *B. subtilis* strains containing fluorescent

557 reporters were grown at 30 °C on the biofilm-inducing medium MSgg for 48 h.

558 Brightness was linearly adjusted in the same way for each image using Fiji. Bar, 1 mm

559

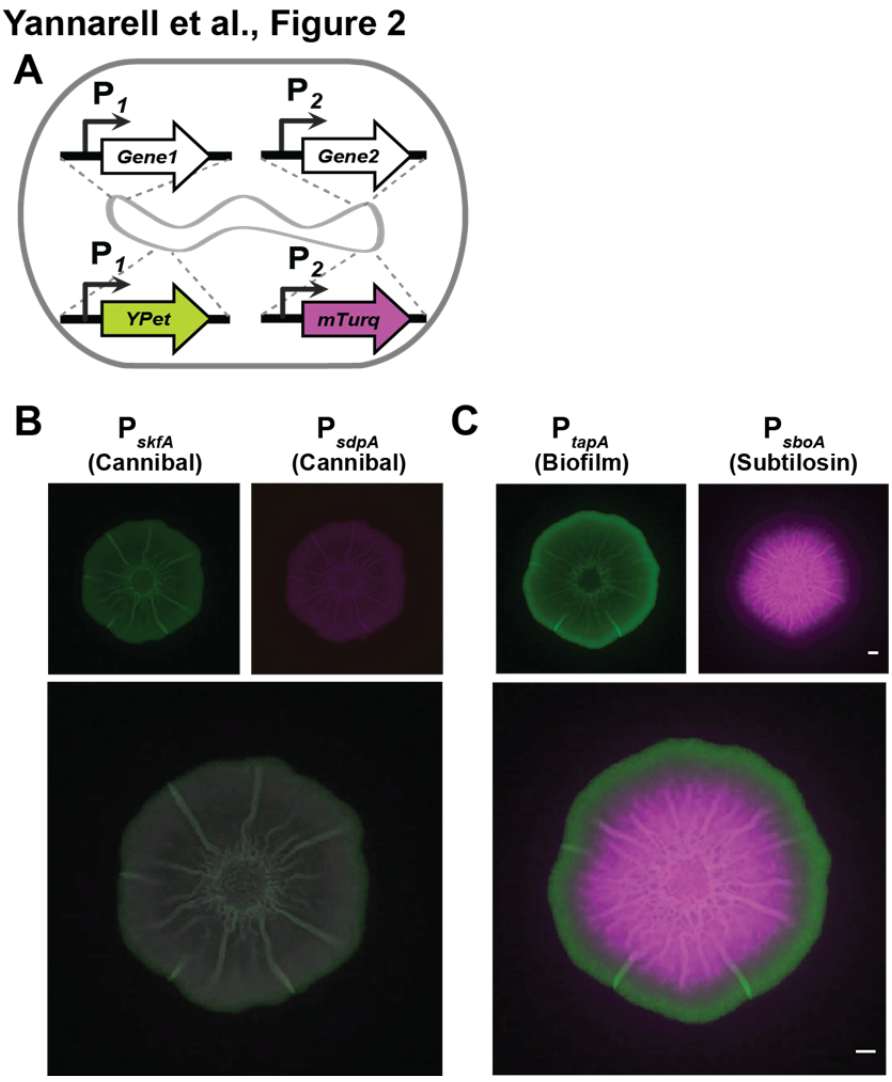

Figure 2. *B. subtilis* double reporters allow for direct localization comparison.

A) Double reporter construction schematic B) Individual and merged channels of a *B. subtilis* biofilm containing *sdpA* (cannibal) and *skfA* (cannibal) reporters and C) a *B. subtilis* biofilm containing *tapA* (biofilm) and *sboA* (subtilosin) reporters grown on MSgg for 48 h. Colony images were taken from the top using a dissecting stereomicroscope. Bars, 1 mm.

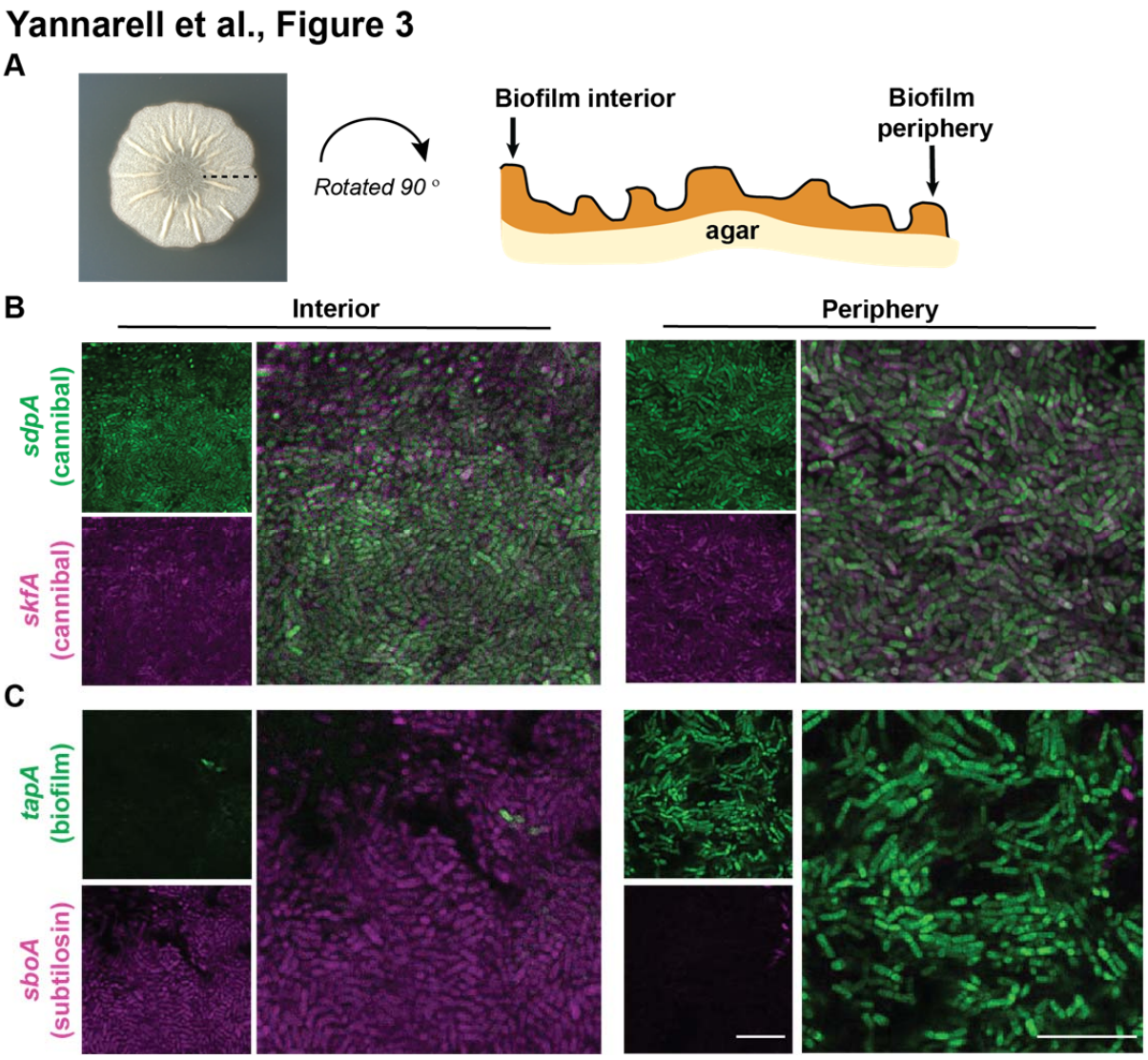

Figure 3. Specific phenotypic reporters display regions of co-localization and regions of distinct expression. A) Schematic of *B. subtilis* biofilm thin-section. B) Micrographs showing individual and merged channels of a *B. subtilis* biofilm containing *sdpA* (cannibal) and *skfA* (cannibal) reporters and C) *B. subtilis* biofilm containing *tapA* (biofilm) and *sboA* (subtilosin) grown on MSgg for 48 h, thin-sectioned, and imaged using Airyscan confocal microscopy at 100X to image interior and periphery regions. For each reporter pair, the intensities were optimized to show differences between reporters (i.e., intensities of B and C are not comparable). Bars, 10 um.

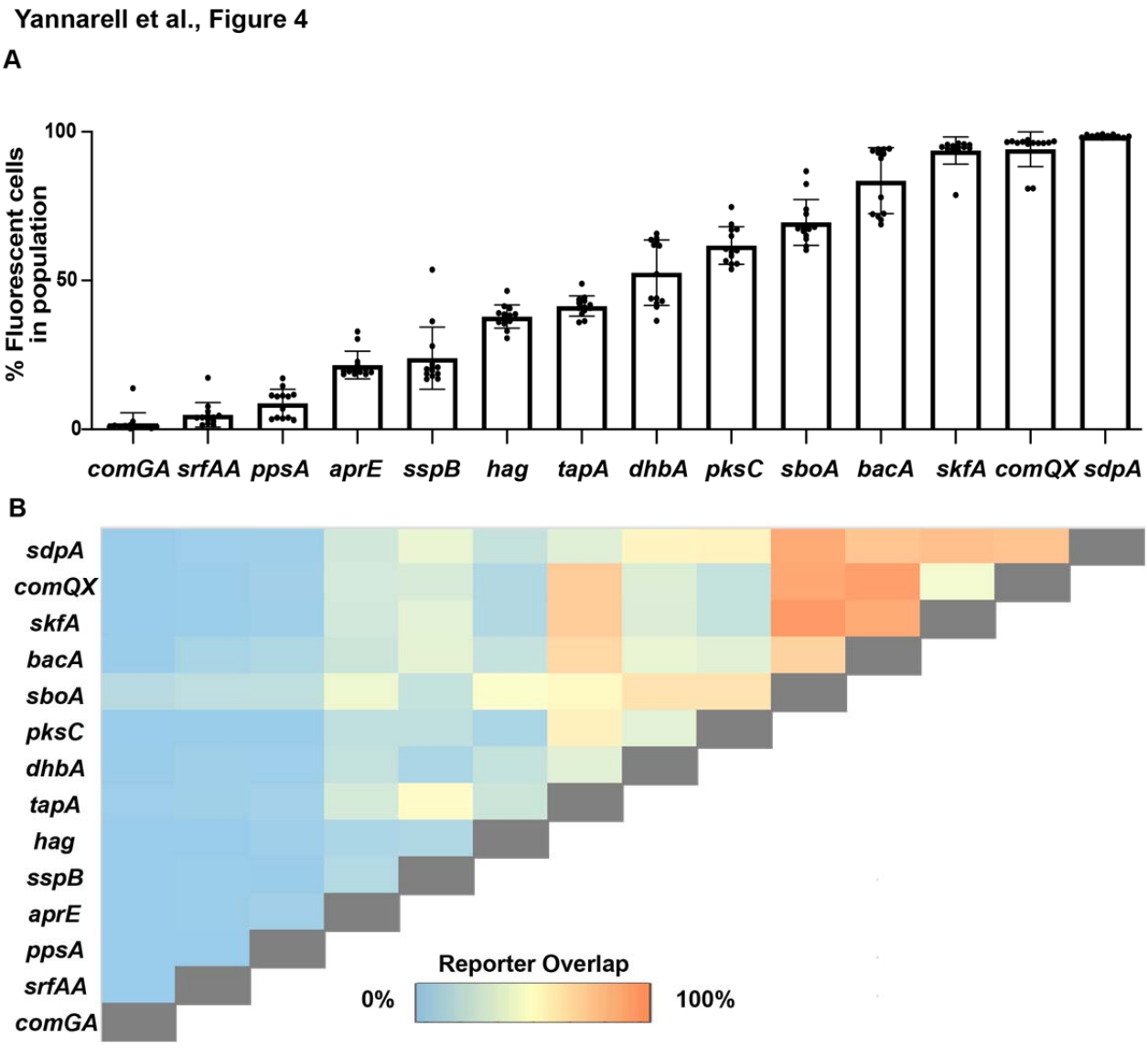

Figure 4. Many *B. subtilis* genes exhibit co-expression at the individual cell-level. A) Percent of fluorescent cells in a *B. subtilis* biofilm population after 48 h growth on MSgg was determined by flow cytometry. B) The percentage of cells co-expressing two reporters after 48 h growth on MSgg.

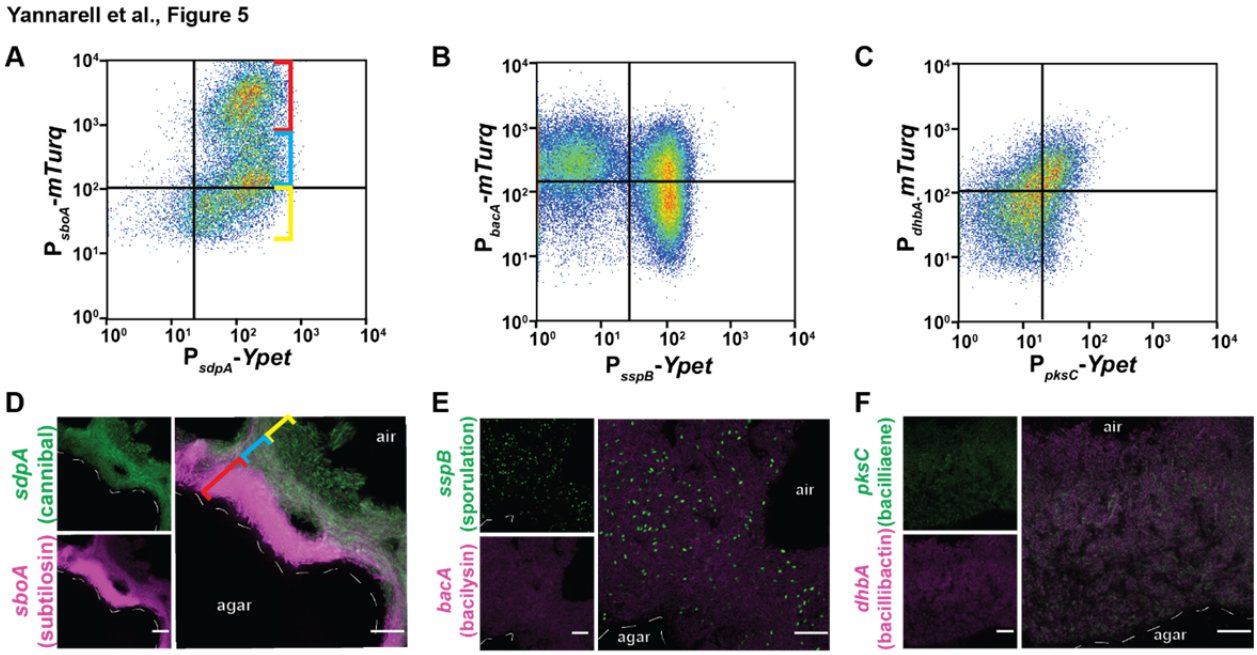

585

586 **Figure 5. Corresponding reporter spatial arrangement with relationships**

587 **displayed in flow cytometry data**. Flow cytometry of the fluorescent intensities of *B.*

588 *subtilis* cells containing A) *sdpA* and *sboA*, B) *sspB* and *bacA*, and C) *dhbA* and pksC

589 reporters harvested from the 48 h timepoint. The gates were constructed from the non-

590 fluorescent control sample from that experiment. A total of 24,000 cells were quantified

591 for each sample. The *mTurq* reporter was detected using a 457 nm laser, and the *Ypet*

592 reporter was detected using a 488 nm laser. Confocal microscopy of *B. subtilis* biofilm

593 thin-sections containing D) *sdpA* and *sboA*, E) *sspB* and *bacA*, and F) *dhbA* and pksC

594 reporters at 100X. For D and E, propyl gallate mounting medium was used. For each

595 reporter pair, the intensities were optimized to show differences between reporters.

596 Bars, 10um.

597

598

599

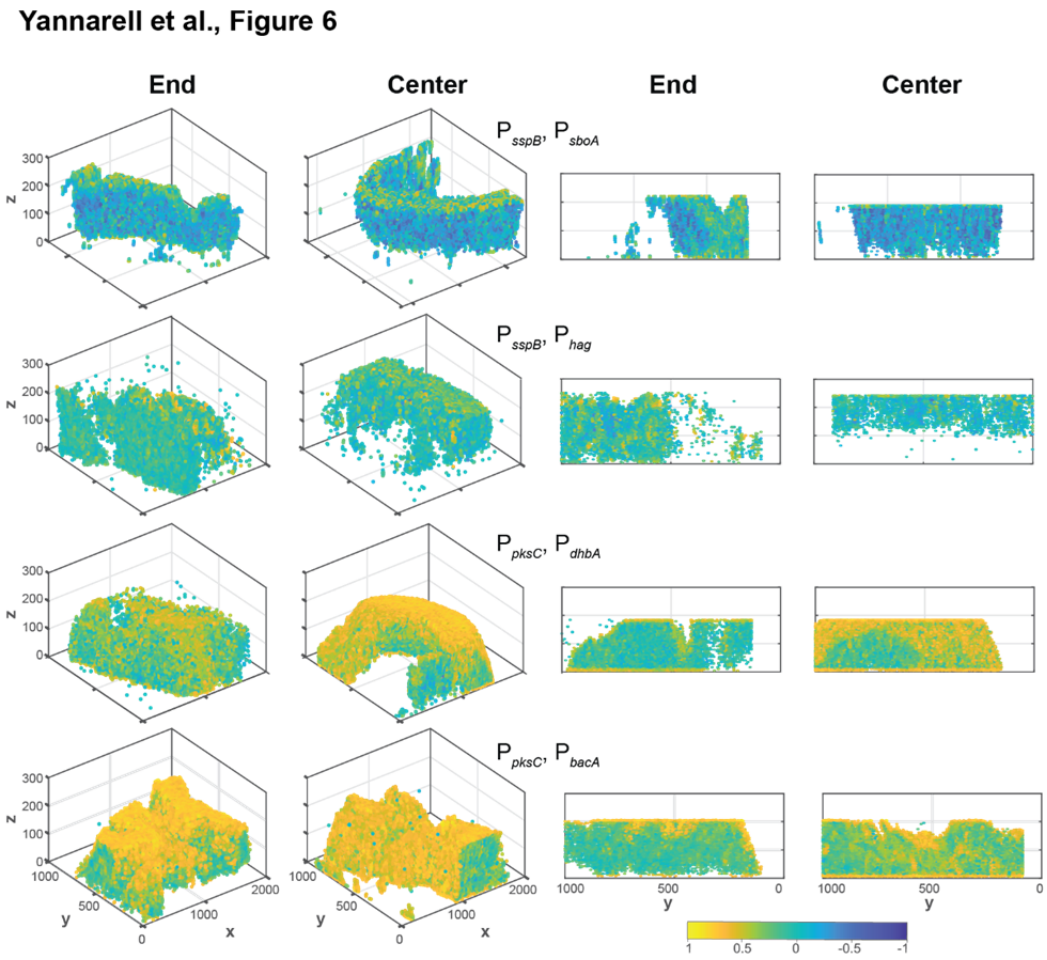

Figure 6. Correlations between pairs of reporters from confocal microscopy. Pearson correlation coefficients were determined between the fluorescent intensities of the two genes expressed in the dual-reporter strains of *B. subtilis*; the reporters are indicated for each row (ES338, ES329, ES392, and ES393). “End” indicates the peripheral, outer edge of the colony while “Center” indicates the center of the biofilm colony. The left two panels are three-dimensional representations of the colony slice and the right two panels are cross-sections of these images. Yellow indicates highly correlated fluorescence between the two reporters within each strain, while dark blue indicates anti-correlated fluorescence. Areas with no fluorescence are not represented in these images.

611 **SUPPLEMENTAL MATERIAL**

612

613 **Table S1.**

614 Table S1 lists the strains used in this study.

615

616 **Figure S1.** Colony morphology of *B. subtilis* wild-type and *B. subtilis* P_{sunA}-*Ypet* grown
617 at 30°C on the biofilm-inducing medium MSgg for 48 h. Colony images were taken from
618 the top using a dissecting stereomicroscope. Bar, 1 mm.

619

620

621 **Figure S2 .** Average fluorescent pixel intensity of *B. subtilis* biofilms containing single
622 *Ypet* reporters depicted in Figure 1. Intensity is plotted (black line) from the center (x-
623 axis = 0) to the edge of the colony (x-axis = 100). The baseline autofluorescence
624 detected in the agar is displayed by the dashed red line. 95% confidence intervals are
625 indicated by grey dashed lines.

626

627

628 **Figure S3.** Growth of wild-type and a representative subset of single and double
629 reporter *B. subtilis* strains measured by OD_{600} measurements over time. Baseline
630 corrected using blank MSgg medium.

631

632 **Figure S4.** Flow cytometry profiles of *B. subtilis* reporters pairs.

633

REFERENCES

1. Ackermann M. 2015. A functional perspective on phenotypic heterogeneity in microorganisms. Nature Reviews Microbiology 13:497-508.
2. Schreiber F, Littmann S, Lavik G, Escrig S, Meibom A, Kuypers MMM, Ackermann M. 2016. Phenotypic heterogeneity driven by nutrient limitation promotes growth in fluctuating environments. Nature Microbiology 1:16055.
3. Heyse J, Buysschaert B, Props R, Rubbens P, Skirtach AG, Waegeman W, Boon N. 2019. Coculturing bacteria leads to reduced phenotypic heterogeneities. Applied and Environmental Microbiology 85.
4. Sturm A, Dworkin J. 2015. Phenotypic diversity as a mechanism to exit cellular dormancy. Current Biology 25:2272-2277.
5. Donaldson GP, Chou W-C, Manson AL, Rogov P, Abeel T, Bochicchio J, Ciulla D, Melnikov A, Ernst PB, Chu H, Giannoukos G, Earl AM, Mazmanian SK. 2020. Spatially distinct physiology of Bacteroides fragilis within the proximal colon of gnotobiotic mice. Nature Microbiology 5:746-756.
6. Veening JW, Smits WK, Kuipers OP. 2008. Bistability, epigenetics, and bet-hedging in bacteria. Annu Rev Microbiol 62:193-210.
7. Gefen O, Balaban NQ. 2009. The importance of being persistent: heterogeneity of bacterial populations under antibiotic stress. FEMS Microbiology Reviews 33:704-717.
8. West SA, Cooper GA. 2016. Division of labour in microorganisms: an evolutionary perspective. Nature Reviews Microbiology 14:716-723.
9. Ren Y, Wang C, Chen Z, Allan E, Mei HCvd, Busscher HJ. 2018. Emergent heterogeneous microenvironments in biofilms: substratum surface heterogeneity and bacterial adhesion force-sensing. FEMS Microbiology Reviews 42:259-272.
10. Armbruster CR, Lee CK, Parker-Gilham J, de Anda J, Xia A, Zhao K, Murakami K, Tseng BS, Hoffman LR, Jin F, Harwood CS, Wong GCL, Parsek MR. 2019. Heterogeneity in surface sensing suggests a division of labor in Pseudomonas aeruginosa populations. eLife 8:e45084.
11. Davis KM, Isberg RR. 2018. One for all, but not all for one: Social behavior during bacterial diseases. Trends in Microbiology 27:64-74.
12. Desai SK, Kenney LJ. 2019. Switching lifestyles is an in vivo adaptive strategy of bacterial pathogens. Frontiers in Cellular and Infection Microbiology 9:421.
13. Reyes Ruiz LM, Williams CL, Tamayo R. 2020. Enhancing bacterial survival through phenotypic heterogeneity. PLoS Pathog 16:e1008439.
14. Evans CR, Kempes CP, Price-Whelan A, Dietrich LEP. 2020. Metabolic heterogeneity and cross-feeding in bacterial multicellular systems. Trends in Microbiology 28:732-743.
15. Nikolic N, Schreiber F, Co AD, Kiviet DJ, Bergmiller T, Littmann S, Kuypers MMM, Ackermann M. 2017. Cell-to-cell variation and specialization in sugar metabolism in clonal bacterial populations. PLOS Genetics 13:e1007122.
16. Rosenthal AZ, Qi Y, Hormoz S, Park J, Li SH, Elowitz MB. 2018. Metabolic interactions between dynamic bacterial subpopulations. Elife 7.
17. Co AD, Vliet Sv, Ackermann M. 2019. Emergent microscale gradients give rise to metabolic cross-feeding and antibiotic tolerance in clonal bacterial populations. Philosophical Transactions of the Royal Society B 374:20190080.
18. Liu J, Prindle A, Humphries J, Gabalda-Sagarra M, Asally M, Lee DY, Ly S, Garcia-Ojalvo J, Suel GM. 2015. Metabolic co-dependence gives rise to collective oscillations within biofilms. Nature 523:550-4.
19. Dietrich LEP, Okegbe C, Price-Whelan A, Sakhtah H, Hunter RC, Newman DK. 2013. Bacterial community morphogenesis is intimately linked to the intracellular redox state. Journal of Bacteriology 195:1371-1380.

20. Schiessl KT, Hu F, Jo J, Nazia SZ, Wang B, Price-Whelan A, Min W, Dietrich LEP. 2019. Phenazine production promotes antibiotic tolerance and metabolic heterogeneity in Pseudomonas aeruginosa biofilms. Nature Communications 10:762.
21. Dragos A, Kiesewalter H, Martin M, Hsu CY, Hartmann R, Wechsler T, Eriksen C, Brix S, Drescher K, Stanley-Wall N, Kummerli R, Kovacs AT. 2018. Division of Labor during Biofilm Matrix Production. Curr Biol 28:1903-1913 e5.
22. Veening JW, Igoshin OA, Eijlander RT, Nijland R, Hamoen LW, Kuipers OP. 2008. Transient heterogeneity in extracellular protease production by Bacillus subtilis. Molecular Systems Biology 4:184.
23. López D, Vlamakis H, Losick R, Kolter R. 2009. Cannibalism enhances biofilm development in Bacillus subtilis. Molecular Microbiology 74:609-618.
24. Gestel Jv, Vlamakis H, Kolter R. 2015. From cell differentiation to cell collectives: Bacillus subtilis uses division of labor to migrate. PLoS Biology 13:e1002141-e1002141.
25. Beauregard PB, Chai Y, Vlamakis H, Losick R, Kolter R. 2013. Bacillus subtilis biofilm induction by plant polysaccharides. Proc Natl Acad Sci U S A 110:E1621-30.
26. Stewart PS, Franklin MJ. 2008. Physiological heterogeneity in biofilms. Nature Reviews Microbiology 6:199-210.
27. Vlamakis H, Chai Y, Beauregard P, Losick R, Kolter R. 2013. Sticking together: building a biofilm the Bacillus subtilis way. Nature Reviews Microbiology 11:157-168.
28. Lopez D, Vlamakis H, Kolter R. 2009. Generation of multiple cell types in Bacillus subtilis. FEMS Microbiology Reviews 33:152-163.
29. Vlamakis H, Aguilar C, Losick R, Kolter R. 2008. Control of cell fate by the formation of an architecturally complex bacterial community. Genes and Development 22:945-953.
30. López D, Vlamakis H, Losick R, Kolter R. 2009. Paracrine signaling in a bacterium. Genes & Development 23:1631-1638.
31. Chai Y, Norman T, Kolter R, Losick R. 2010. An epigenetic switch governing daughter cell separation in Bacillus subtilis. Genes & Development 24:754-765.
32. van Gestel J, Vlamakis H, Kolter R. 2015. From cell differentiation to cell collectives: Bacillus subtilis uses division of labor to migrate. PLoS Biol 13:e1002141.
33. She Q, Hunter E, Qin Y, Nicolau S, Zalis EA, Wang H, Chen Y, Chai Y. 2020. Negative interplay between biofilm formation and competence in the environmental strains of Bacillus subtilis. mSystems 5.
34. Steinberg N, Keren-Paz A, Hou Q, Doron S, Yanuka-Golub K, Olender T, Hadar R, Rosenberg G, Jain R, Cámara-Almirón J, Romero D, Teeffelen Sv, Kolodkin-Gal I. 2020. The extracellular matrix protein TasA is a developmental cue that maintains a motile subpopulation within Bacillus subtilis biofilms. Science Signaling 13:eaaw8905.
35. Marlow VL, Cianfanelli FR, Porter M, Cairns LS, Dale JK, Stanley-Wall NR. 2014. The prevalence and origin of exoprotease-producing cells in the Bacillus subtilis biofilm. Microbiology (Reading) 160:56-66.
36. Lopez D, Vlamakis H, Kolter R. 2009. Generation of multiple cell types in Bacillus subtilis. FEMS Microbiology Reviews 33:152-163.
37. González-Pastor JE. 2011. Cannibalism: a social behavior in sporulating Bacillus subtilis. FEMS Microbiology Reviews 35:415-424.
38. Kaspar F, Neubauer P, Gimpel M. 2019. Bioactive Secondary Metabolites from Bacillus subtilis: A Comprehensive Review. J Nat Prod 82:2038-2053.
39. Schoenborn AA, Yannarell SM, Wallace ED, Clapper H, Weinstein IC, Shank EA. 2021. Defining the Expression, Production, and Signaling Roles of Specialized Metabolites during Bacillus subtilis Differentiation. Journal of Bacteriology 203:e00337-21.

40. Lopez D, Fischbach MA, Chu F, Losick R, Kolter R. 2009. Structurally diverse natural products that cause potassium leakage trigger multicellularity in Bacillus subtilis. Proc Natl Acad Sci U S A 106:280-5.
41. Dubnau D. 1991. The regulation of genetic competence in Bacillus subtilis. Molecular Microbiology 5:11-18.
42. Magnuson R, Solomon J, Grossman AD. 1994. Biochemical and genetic characterization of a competence pheromone from B. subtilis. Cell 77:207-216.
43. Lamsa A, Liu WT, Dorrestein PC, Pogliano K. 2012. The Bacillus subtilis cannibalism toxin SDP collapses the proton motive force and induces autolysis. Mol Microbiol 84:486-500.
44. Grandchamp GM, Caro L, Shank EA. 2017. Pirated Siderophores Promote Sporulation in Bacillus subtilis. Appl Environ Microbiol 83.
45. Strauch MA, Bobay BG, Cavanagh J, Yao F, Wilson A, Le Breton Y. 2007. Abh and AbrB control of Bacillus subtilis antimicrobial gene expression. J Bacteriol 189:7720-32.
46. Inaoka T, Wang G, Ochi K. 2009. ScoC regulates bacilysin production at the transcription level in Bacillus subtilis. J Bacteriol 191:7367-71.
47. Romero D, Aguilar C, Losick R, Kolter R. 2010. Amyloid fibers provide structural integrity to Bacillus subtilis biofilms. Proc Natl Acad Sci U S A 107:2230-4.
48. Inaoka T, Ochi K. 2011. Scandium Stimulates the Production of Amylase and Bacilysin in Bacillus subtilis. Applied and Environmental Microbiology 77:8181-8183.
49. Vargas-Bautista C, Rahlwes K, Straight P. 2014. Bacterial competition reveals differential regulation of the pks genes by Bacillus subtilis. J Bacteriol 196:717-28.
50. Yannarell SM, Velickovic D, Anderton CR, Shank EA. 2021. Direct Visualization of Chemical Cues and Cellular Phenotypes throughout Bacillus subtilis Biofilms. mSystems 6:e0103821.
51. Aguilar C, Vlamakis H, Guzman A, Losick R, Kolter R. 2010. KinD Is a Checkpoint Protein Linking Spore Formation to Extracellular-Matrix Production in Bacillus subtilis Biofilms. mBio 1:e00035-10.
52. Shimotsu H, Henner DJ. 1986. Construction of a single-copy integration vector and its use in analysis of regulation of the trp operon of Bacillus subtilis. Gene 43:85-94.
53. Branda SS, Gonzalez-Pastor JE, Ben-Yehuda S, Losick R, Kolter R. 2001. Fruiting body formation by Bacillus subtilis. Proc Natl Acad Sci U S A 98:11621-6.
54. Hartl B, Wehrl W, Wiegert T, Homuth G, Schumann W. 2001. Development of a new integration site within the Bacillus subtilis chromosome and construction of compatible expression cassettes. J Bacteriol 183:2696-9.
55. López D, Vlamakis H, Losick R, Kolter R. 2009. Cannibalism enhances biofilm development in Bacillus subtilis. Molecular Microbiology 74:609-618.
56. Veening J-W, Stewart EJ, Berngruber TW, Taddei F, Kuipers OP, Hamoen LW. 2008. Bet-hedging and epigenetic inheritance in bacterial cell development. Proceedings of the National Academy of Sciences 105:4393-4398.
57. Lopez-Garrido J, Ojkic N, Khanna K, Wagner FR, Villa E, Endres RG, Pogliano K. 2018. Chromosome Translocation Inflates Bacillus Forespores and Impacts Cellular Morphology. Cell 172:758-770.e14.
58. Hartmann R, Jeckel H, Jelli E, Singh PK, Vaidya S, Bayer M, Rode DKH, Vidakovic L, Díaz-Pascual F, Fong JCN, Dragoš A, Lamprecht O, Thöming JG, Netter N, Häussler S, Nadell CD, Sourjik V, Kovács ÁT, Yildiz FH, Drescher K. 2021. Quantitative image analysis of microbial communities with BiofilmQ. Nature Microbiology 6:151-156.
59. Nicolas P, Mäder U, Dervyn E, Rochat T, Leduc A, Pigeonneau N, Bidnenko E, Marchadier E, Hoebeke M, Aymerich S, Becher D, Bisicchia P, Botella E, Delumeau O, Doherty G, Denham EL, Fogg MJ, Fromion V, Goelzer A, Hansen A, Härtig E, Harwood CR, Homuth G, Jarmer H, Jules M, Klipp E, Chat LL, Lecointe F, Lewis P, Liebermeister

W, March A, Mars RAT, Nannapaneni P, Noone D, Pohl S, Rinn B, Rügheimer F, Sappa PK, Samson F, Schaffer M, Schwikowski B, Steil L, Stülke J, Wiegert T, Devine KM, Wilkinson AJ, Dijl JMv, Hecker M, Völker U, Bessières P, et al. 2012. Condition-dependent transcriptome reveals high-level regulatory architecture in Bacillus subtilis. Science 335:1103-1106.

60. Arrieta-Ortiz ML, Hafemeister C, Bate AR, Chu T, Greenfield A, Shuster B, Barry SN, Gallitto M, Liu B, Kacmarczyk T, Santoriello F, Chen J, Rodrigues CDA, Sato T, Rudner DZ, Driks A, Bonneau R, Eichenberger P. 2015. An experimentally supported model of the Bacillus subtilis global transcriptional regulatory network. Molecular Systems Biology 11:839.

61. Boonstra M, Schaffer M, Sousa J, Morawska L, Holsappel S, Hildebrandt P, Sappa PK, Rath H, de Jong A, Lalk M, Mader U, Volker U, Kuipers OP. 2020. Analyses of competent and non-competent subpopulations of Bacillus subtilis reveal yhfW, yhxC and ncRNAs as novel players in competence. Environ Microbiol 22:2312-2328.

62. Perego M. 2013. Forty years in the making: understanding the molecular mechanism of peptide regulation in bacterial development. PLoS Biology 11:e1001516.

63. Townsley L, Yannarell SM, Huynh TN, Woodward JJ, Shank EA. 2018. Cyclic di-AMP acts as an extracellular signal that impacts Bacillus subtilis biofilm formation and plant attachment. mBio 9:e00341-18.

64. Weiss CA, Hoberg JA, Liu K, Tu BP, Winkler WC. 2019. Single-cell microscopy reveals that levels of cyclic di-GMP vary among Bacillus subtilis subpopulations. Journal of Bacteriology 201.

65. Kobayashi K, Ikemoto Y. 2019. Biofilm-associated toxin and extracellular protease cooperatively suppress competitors in Bacillus subtilis biofilms. PLOS Genetics 15:e1008232.

66. Stacy A, McNally L, Darch SE, Brown SP, Whiteley M. 2016. The biogeography of polymicrobial infection. Nat Rev Microbiol 14:93-105.

67. Burmolle M, Ren D, Bjarnsholt T, Sorensen SJ. 2014. Interactions in multispecies biofilms: do they actually matter? Trends Microbiol 22:84-91.

68. Tolker-Nielsen T, Molin S. 2000. Spatial Organization of Microbial Biofilm Communities. Microb Ecol 40:75-84.

69. Bridier A, Piard JC, Pandin C, Labarthe S, Dubois-Brissonnet F, Briandet R. 2017. Spatial Organization Plasticity as an Adaptive Driver of Surface Microbial Communities. Front Microbiol 8:1364.

70. Liu W, Roder HL, Madsen JS, Bjarnsholt T, Sorensen SJ, Burmolle M. 2016. Interspecific Bacterial Interactions are Reflected in Multispecies Biofilm Spatial Organization. Front Microbiol 7:1366.

71. Liu W, Jacquiod S, Brejnrod A, Russel J, Burmolle M, Sorensen SJ. 2019. Deciphering links between bacterial interactions and spatial organization in multispecies biofilms. ISME J 13:3054-3066.

72. Ferrer MD, Mira A. 2016. Oral Biofilm Architecture at the Microbial Scale. Trends Microbiol 24:246-248.

73. Elowitz MB, Levine AJ, Siggia ED, Swain PS. 2002. Stochastic gene expression in a single cell. Science 297:1183-6.

74. Nadezhdin E, Murphy N, Dalchau N, Phillips A, Locke JCW. 2020. Stochastic pulsing of gene expression enables the generation of spatial patterns in Bacillus subtilis biofilms. Nature Communications 11:950.

75. Grubbs KJ, Bleich RM, Santa Maria KC, Allen SE, Farag S, AgBiome T, Shank EA, Bowers AA. 2017. Large-Scale Bioinformatics Analysis of Bacillus Genomes Uncovers Conserved Roles of Natural Products in Bacterial Physiology. mSystems 2.

76. Gavriilidou A, Kautsar SA, Zaburannyi N, Krug D, Müller R, Medema MH, Ziemert N. 2022. Compendium of specialized metabolite biosynthetic diversity encoded in bacterial genomes. Nat Microbiol 7:726-735.
77. Schoenborn AA, Yannarell SM, Wallace ED, Clapper H, Weinstein IC, Shank EA. 2021. Defining the Expression, Production, and Signaling Roles of Specialized Metabolites during Bacillus subtilis Differentiation. J Bacteriol 203:e0033721.
78. Shank EA, Klepac-Ceraj V, Collado-Torres L, Powers GE, Losick R, Kolter R. 2011. Interspecies interactions that result in Bacillus subtilis forming biofilms are mediated mainly by members of its own genus. Proceedings of the National Academy of Sciences 108:E1236-E1243.
79. Powers MJ, Sanabria-Valentín E, Bowers AA, Shank EA. 2015. Inhibition of Cell Differentiation in Bacillus subtilis by Pseudomonas protegens. Journal of Bacteriology 197:2129-2138.
80. Yasbin RE, Young FE. 1974. Transduction in Bacillus subtilis by bacteriophage SPP1. J Virol 14:1343-8.
81. Yannarell SM, Grandchamp GM, Chen SY, Daniels KE, Shank EA. 2019. A Dual-Species Biofilm with Emergent Mechanical and Protective Properties. J Bacteriol 201.
82. Sharma K, Palatinszky M, Nikolov G, Berry D, Shank EA. 2020. Transparent soil microcosms for live-cell imaging and non-destructive stable isotope probing of soil microorganisms. Elife 9.
83. Gibson DG, Young L, Chuang R-Y, Venter JC, Hutchison CA, Smith HO. 2009. Enzymatic assembly of DNA molecules up to several hundred kilobases. Nature Methods 6:343-345.
84. Doan T, Marquis KA, Rudner DZ. 2005. Subcellular localization of a sporulation membrane protein is achieved through a network of interactions along and across the septum. Molecular Microbiology 55:1767-1781.
85. Jones BV, Young R, Mahenthiralingam E, Stickler DJ. 2004. Ultrastructure of Proteus mirabilis swarmer cell rafts and role of swarming in catheter-associated urinary tract infection. Infection and immunity 72:3941-3950.

Yannarell et al., Figure 1

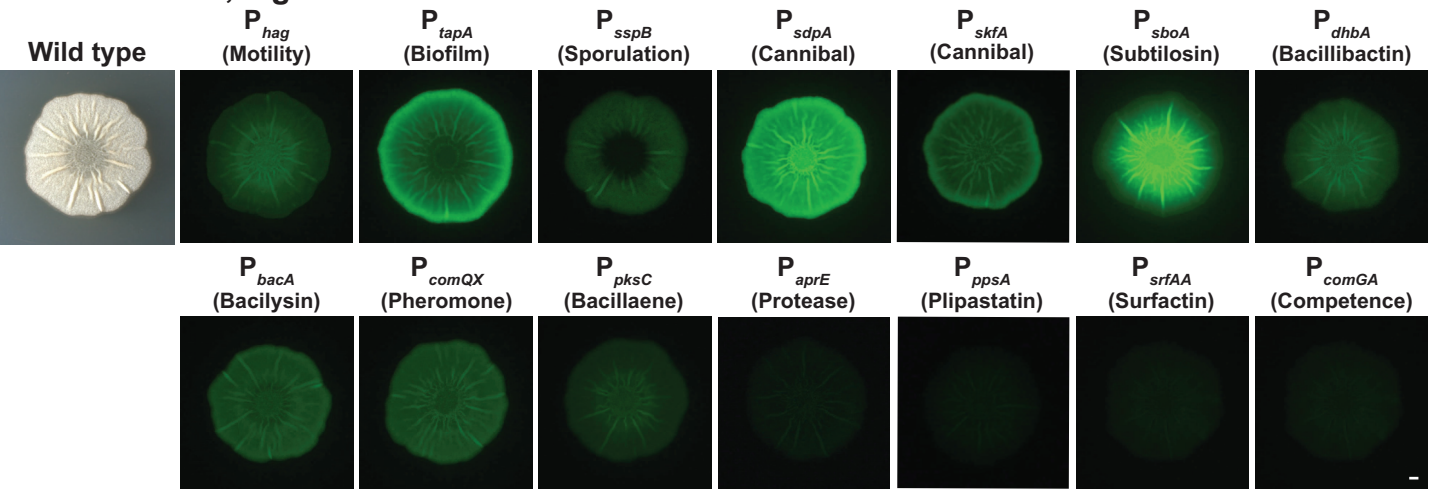

Yannarell et al., Figure 2

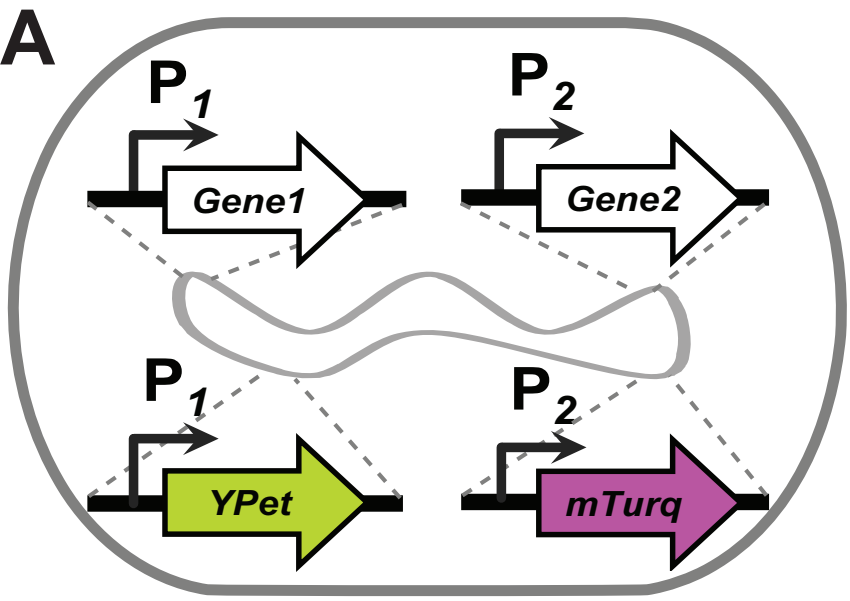

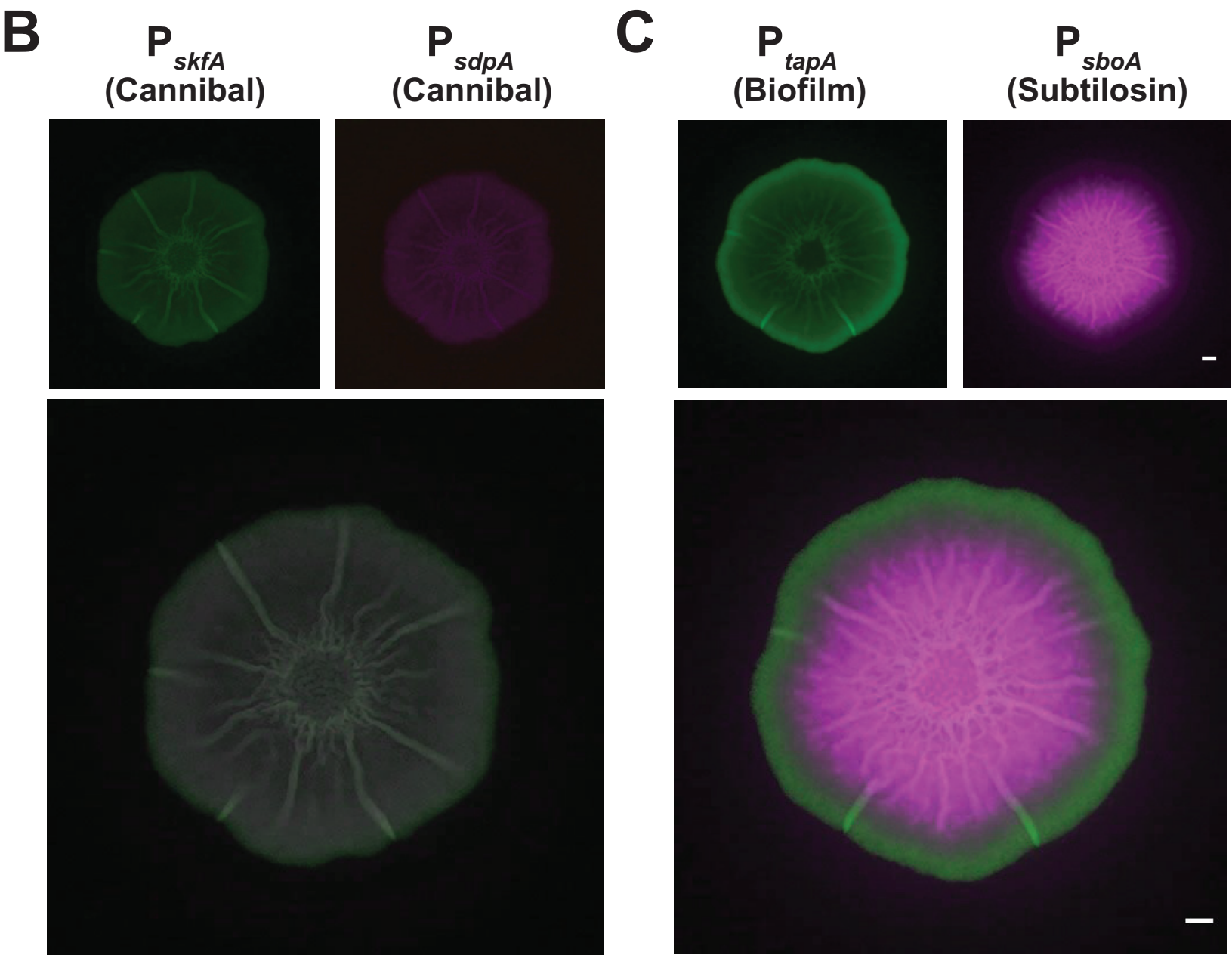

Yannarell et al., Figure 3

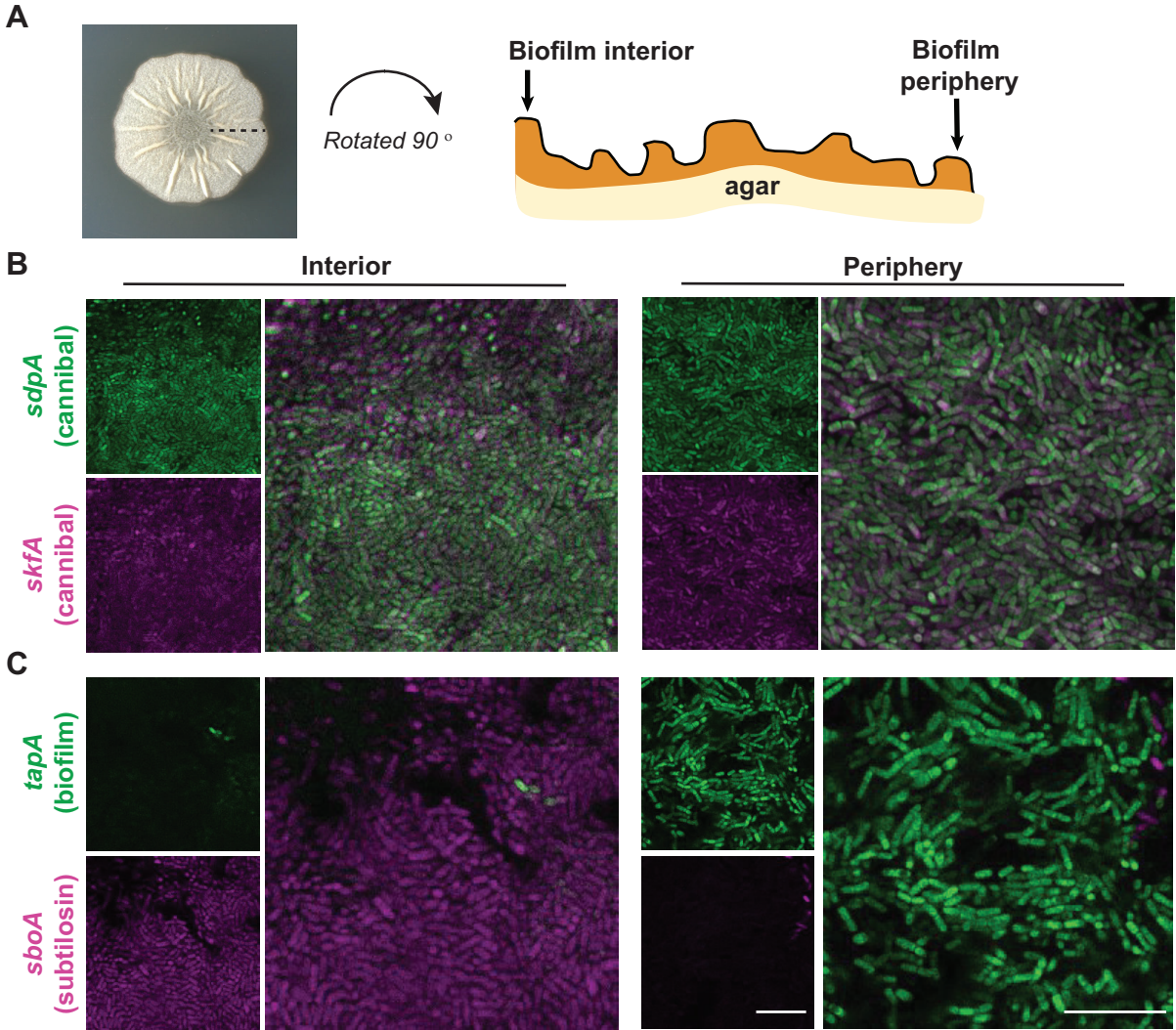

Yannarell et al., Figure 4

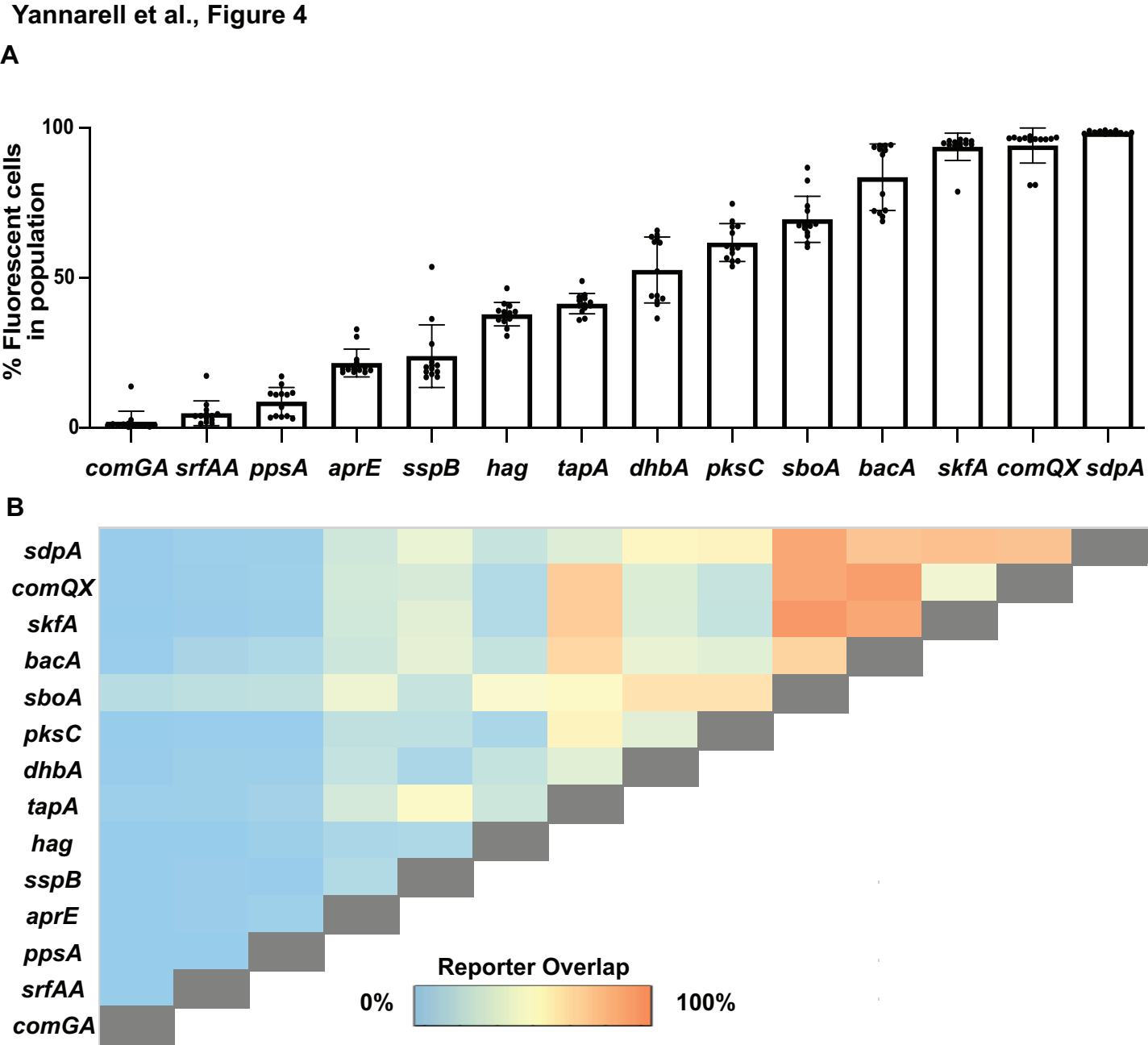

Yannarell et al., Figure 5

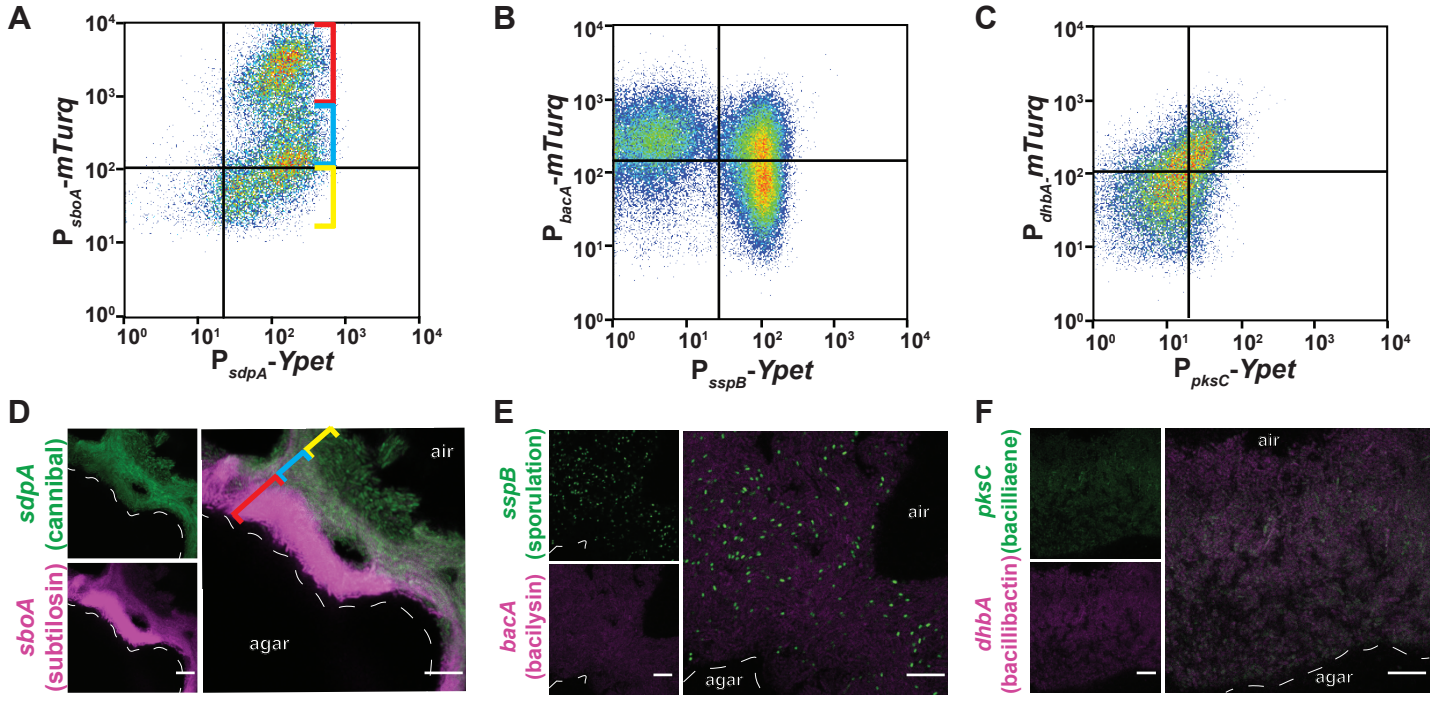

Yannarell et al., Figure 6